Journal of Enzymes

Disruption of Hydrogen Bonding Network Decreases Catalytic Diversity of Chloroperoxidase via Abolishing Both Chlorination and Dismutation Activities

Elena Shersher[1], Armando D. Pardillo[1], Xiaotang Wang[1,*]

[1]Department of Chemistry and Biochemistry, Florida International University, Miami, FL 33199, USA

Research Article

Open Access &

Peer-Reviewed Article

DOI: 10.14302/issn.2690-4829.jen-24-5291

Running title:

Proximal hydrogen bonding network of chloroperoxidase

Corresponding author:

Xiaotang Wang, Department of Chemistry and Biochemistry, Florida International University, Miami, FL 33199, USA

Keywords:

chloroperoxidase, heme enzyme, halogenation, peroxidation, epoxidation, hydrogen peroxide dismutation, hydrogen bond network, catalysis

Received: September 07, 2024

Accepted: October 19, 2024

Published: November 01, 2024

Citation:

Elena Shersher, Armando D. Pardillo, Xiaotang Wang (2024) Disruption of Hydrogen Bonding Network Decreases Catalytic Diversity of Chloroperoxidase via Abolishing Both Chlorination and Dismutation Activities. Journal of Enzymes - 1(3):13-33. https://doi.org/10.14302/issn.2690-4829.jen-24-5291

Abstract

The perpendicular orientation of the proximal alpha helix to the heme plane in chloroperoxidase (CPO) maximizes the influence of its intrinsic helix dipole that has been shown to reduce the "push-effect", thereby increasing the heme redox potential and fine-tuning the catalytic capabilities of CPO. We investigated the effects of a disruption of the hydrogen bonding network between R26-N37 and A27-N33, formed by the proximal alpha helix, on the CPO structural stability and catalytic profile using site-directed mutagenesis and spectroscopy. The mutant CPO (R26A, N33A, and R26A/N33A) exhibited significant tertiary structural changes and distinct heme coordination, likely, due to destabilization of the proximal helix as a result of the disruption of the proximal hydrogen bonding network. In line with these observations, biochemical characterizations showed that all mutants displayed dramatically different activity profiles relative to that of the WT CPO. Mutant epoxidation and peroxidation activities were markedly enhanced, especially in the R26A/N33A CPO mutant. Moreover, all mutant CPO enzymes exhibited broader pH profiles in both epoxidation and peroxidation activities, including a shift in the optimal peroxidation activity towards pH 3.5 as opposed to pH 2.75. Conversely, the dismutation activity (pH 3.0-5.5) was almost completely lost while chlorination activity (pH 2.75-5.0) was virtually non-existent in all CPO mutants. Our results demonstrate the important role the R26-N37 and A27-N33 hydrogen bond pairs play in the heme coordination and tertiary structure of CPO defining its catalytic capabilities, and also suggest the importance of the proximal helix stability and orientation.

Introduction

Chloroperoxidase (CPO) from *Calderiomyces fumago* is a heme-thiolate protein that belongs to the peroxidase-peroxygenase family of enzymes.[1,2] Most heme enzymes are capable of efficiently catalyzing only one or two specific types of reactions.[3-5] Chloroperoxidase is special in this regard as it efficiently catalyzes a plethora of reactions including peroxidation, dismutation, halogenation, hydroxylation, and epoxidation.[1,6-8]

The diverse catalytic activity of CPO has long been attributed to its unique active site structure that combines structural features of two different classes of heme

enzymes: peroxidases and cytochromes P450. The active site is comprised of the heme-thiolate (proximally bound Cys29) and a polar distal pocket. The polar pocket is a typical feature of peroxidases but different from the non-polar distal pocket of the P450. Conversely, the proximal Cys ligation is similar to that found in P450 but distinct from the proximal His coordination in traditional peroxidases.[2] The CPO hybrid features have attracted much attention,[2,9-12] as the majority of catalytic activity occurs in the heme pocket. However, significantly less attention has been given to the proximal residues (except Cys29), although prior work has already illuminated their importance.[13,14]

The proximal heme thiolate serves as a strong electron donor that "pushes" electron density toward the heme iron,[15-18] facilitating Compound I (Cpd I) formation,[18-20] reducing the redox potential of the heme, and increasing the distal ligand basicity.[17,18,20,21] To mitigate the redox potential decrease, CPO's Ala31 and Leu32 provide 2 strong amide hydrogen bonds to the sulfur of Cys29, reducing the "push effect".[13,14,19] Additionally, Cys29 is located in the N-terminal helix A[2] that produces a dipole, which further reduces the push effect.[14,22] This helix is almost perpendicular to the heme plane (Figure 1),[2] maximizing the influence of the helix dipole. Interestingly, in P450 and most classical peroxidases, the ligand-containing C-terminal helix is parallel to the heme.[23]

CPO catalysis is accomplished via a variety of pathways, involving the formation of the highly active oxyferryl cation radical, Cpd I.[24] In addition to catalyzing peroxidation via Compound II (Cpd II) formation, CPO Cpd I catalyzes halogenation via the oxo-ferric Compound X (Cpd X), dismutation via the catalase pathway, and oxygen insertion reactions through the epoxidation pathway (Figure 2).[21,24,25] One-electron oxidations (Figure 2A) are believed to occur on the CPO surface[26-29] while two-electron oxidations (Figure 2B) – at its active site.[27,30-32] The observed catalytic diversity of CPO is likely the result of its unique structure and may be altered upon removal of the proximal hydrogen bonds.

We hypothesize that the proximal hydrogen bonds (Figure 1) stabilize the proximal alpha helix

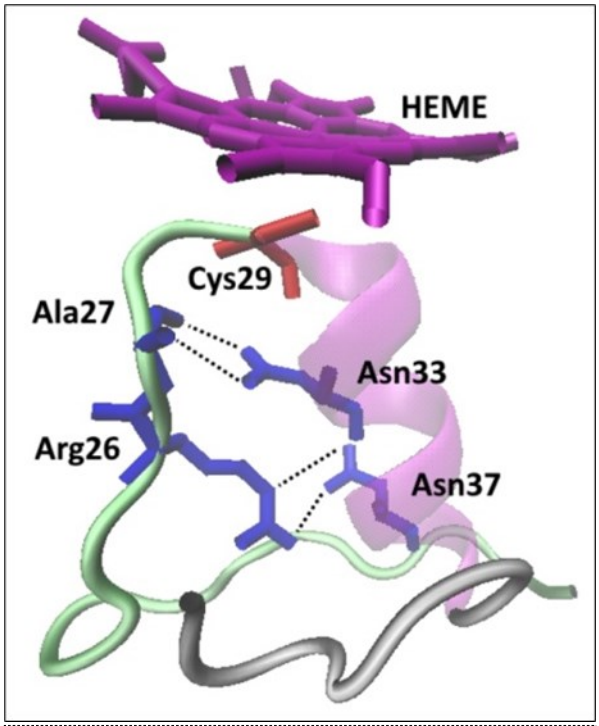

Figure 1. Hydrogen bonding network (Arg26-Asn37 and Ala27-Asn33) in the proximal site of CPO.

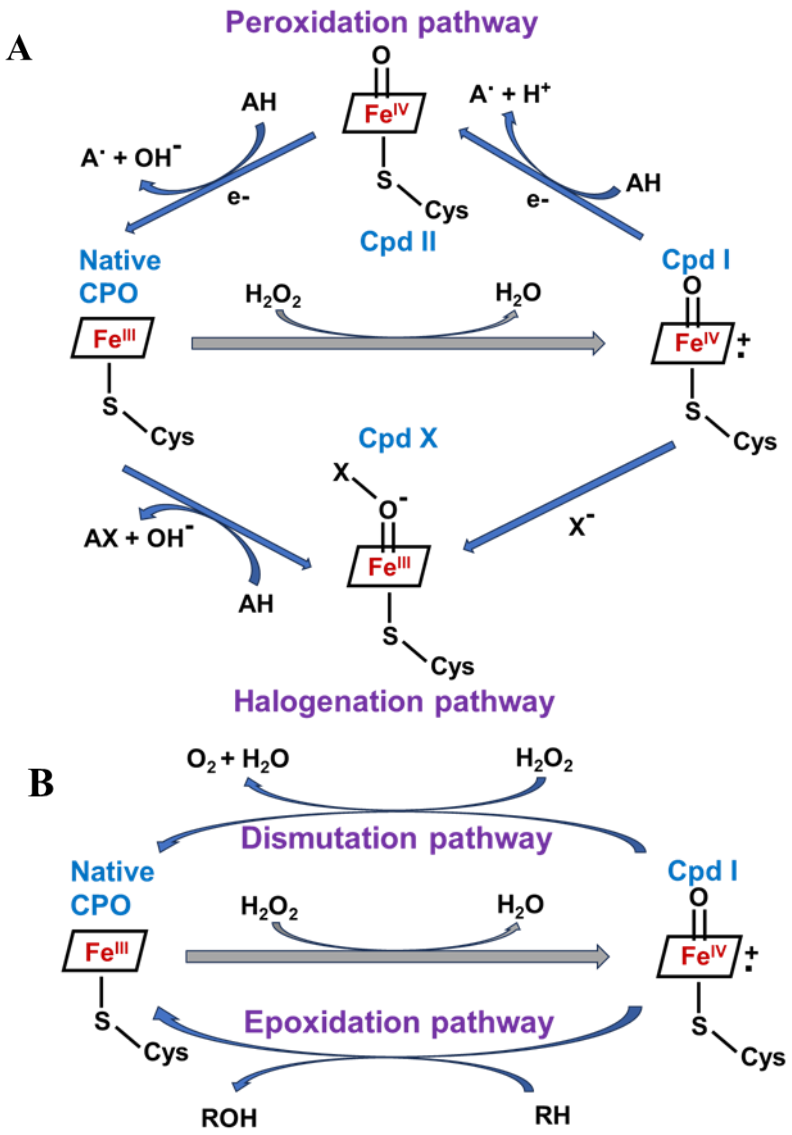

Figure 2. A. One-electron oxidations catalyzed by CPO. B. Two -electron oxidations catalyzed by CPO (adapted from L. P. Hager).

important for CPO's catalytic function, thus significantly influencing the catalytic profile of CPO.[13,14] In this work, we investigated the role of the hydrogen bonding network in modulating the structural, spectroscopic, and catalytic properties of CPO by disrupting the proximal hydrogen bonds. We replaced the R26 and N33 amino acids with Alanine (separately and simultaneously) to disrupt the hydrogen bonds between the R26-N37 and A27-N33 amino acid pairs in CPO. The characterization studies of the resulting mutants R26A, N33A, and R26A/N33A CPO show that the hydrogen bonding network in the proximal helix of CPO not only regulates the spectroscopic signature but also modulates the catalytic profile of CPO.

Materials and Methods

Construction of the R26A, N33A, and R26A/N33A CPO genes

The R26A and N33A mutations were introduced into the pCPO3.I–AmdS (a PUC19-based 13.8-kb plasmid),[33] via a polymerase chain reaction (PCR) amplification using the QuikChange II XL site-directed mutagenesis kit. The PCR reaction was carried out in an Eppendorf thermal cycler (Mastercycler gradient) using PfuUltra HF DNA polymerase. The primers used to introduce the R26A and N33A mutations are listed below:

Coding strain – R26A primer 1 5'- CTACCGACTCT**GCT**GCTCCTTGCCCAGCTCTGAACG - 3'

Non-coding strain – R26A primer 2 5'- GAGCTGGGCAAGGAGC**AGC**AGAGTCGGTAGGAC-CTG - 3'

Coding strain – N33A primer 1 5'- CTTGCCCAGCTCTG**GCC**GCTCTTGCCAACCACGGTT - 3'

Non-coding strain – N33A primer 2 5'- GTTGGCAAGAGC**GGC**CAGAGCTGGGCAAGGAGCAC-GAG - 3'

Coding strain – R26A/N33A primer 1 5'- GTCCTACCGACTCT**GCT**GCTCCTTGCCCAGCTCTGG -3'

Non-coding strain – R26A/N33A primer 2 5'- CAAGGAGC**AGC**AGAGTCGGTAGGAC-CTGGGGCGAC -3'

The plasmid encoding the double mutant was prepared from the plasmid already containing the N33A mutation by introducing the second R26A mutation. The DNA product was digested with Dpn I restriction endonuclease to eliminate the native plasmid. Mutated plasmids were propagated in *E. Coli* (DH5-α strain) with the R26A and N33A mutations confirmed by DNA sequencing (Figure S1).

Transformation of Aspergillus niger with mutant pCPO and mutant selection

The mutant pCPO3.I-AmdS was co-transformed with pAB4-1 (Figure S2) into the *pyrG* mutant (uridine-requiring) protease deficient MGG029 strain of *A. niger* (*prtT gla::fleor pyrG*) using procedures described previously[33,34] with the following modifications. Brown conidiospores were inoculated in 50 mL minimal medium (MM) containing 0.5% yeast extract, 0.5% Casamino acids, 5% maltose, 1% glucose, 70 mM $NaNO_3$, 7 mM KCl, 6 mM KH_2PO_4, 6 mM K_2HPO_4, 2 mM $MgSO_4$, 10 mM uridine, 25 µL of carbenicillin (100 mg/mL stock), 50 µL of the Hutner trace elements solution.[35] The mini-culture was incubated at 250 rpm and 37°C for 1 day and then at 30°C until white-yellow mycelium was observed (2-5 days). After disruption of the mycelium with a homogenizer, the culture was transferred to 1 L MM and incubated at 30°C and 250 rpm for 16-20 hours. Mycelium was collected by filtration through sterile Myracloth followed by protoplast preparation (collected by centrifugation at 3000 rpm, 10 min) and DNA transformation using polyethylene glycol as described previously.[34] Successful transformants were selected on the polyacrylamide plates lacking uridine supplementation and used to express the mutant CPO. Polyacrylamide was used as a source of carbon and nitrogen for growth. Each clone from the acrylamide plates was inoculated in 50 ml MM lacking uridine and yeast extract and incubated at 250 rpm and 22°C for 1 week. The clone with the highest peroxidation activity as determined by 2,2′-azino-bis(3-ethylbenzothiazoline-6-sulfonic acid) (ABTS) assay, was used to set up large-scale protein expression.

Expression and purification of mutant CPO

The *A. niger* spores were inoculated into several 50-mL cultures and grown for 3-4 days at 250 rpm,

25°C. After mycelium homogenization, small cultures were transferred into 4-L flasks containing MM lacking uridine and yeast extract in the presence of 10% fructose, carbenicillin (50 mg/L), and 100 µM δ-aminolevulinic acid (72 L total). Cultures were incubated at 250 rpm and 25°C for 3 days and then at 22°C for 4 more days. Then, the medium was filtered through the glass fiber filter circles G6 and concentrated down to 50 mL in the Amicon stirring pressure cells. The concentrated sample was dialyzed against buffer A (25 mM phosphate buffer, pH 5.9) and filtered through a 0.45 µm membrane. Mutant CPO was purified using an AKTA prime chromatography system. All buffers used during purification were filtered through a 0.45 µm membrane and de-gassed for 15 minutes. The protein sample in buffer A was applied onto a 100-mL column packed with 50 mL of diethylaminoethanol (DEAE) sepharose resin equilibrated with buffer A and eluted with buffer A while gradually increasing NaCl concentration. The R26A and R26A/N33A CPO proteins eluted at approximately 20% 0.5 M NaCl while N33A CPO eluted at 30% 0.5 M NaCl. Fractions with Reinheitzahl (RZ) values (A_{420}/A_{280}) above 0.5 were combined and concentrated down to about 1 mL using a Millipore 30,000 centrifugal filter unit. The sample was filtered through a 0.45 µm membrane and applied onto a gel filtration column containing 500 mL of Sephadex G75 resin and eluted with buffer A. Fractions with RZ values between 1.0 – 1.1 were used in the subsequent studies.

Structural characterization of mutant CPO

Structural characterization of R26A, N33A, and R26A/N33A CPO was performed using a JASCO CD spectrometer and VARIAN UV-Vis spectrophotometer (Cary 300 Bio). The CD spectra of 1 µM mutant and WT CPO in buffer A were collected in the range of 190-260 nm at room temperature using 5-mm quartz cuvettes. Three spectra were averaged for each protein sample. The secondary structures were estimated using the CDSSTR method and reference therein.[36] To evaluate the tertiary structural information of the mutant protein, CD spectra of 16 µM R26A, 35 µM N33A, 11 µM R26A/N33A, and corresponding concentrations of WT CPO in phosphate buffer, pH 5.9 were collected in the range of 250-350 nm at room temperature using 1-cm quartz cuvettes. Three spectra were averaged for each protein sample.

The UV-Vis absorption spectra of the mutant and WT CPO proteins in buffer A were collected from 250-700 nm at room temperature using 1-cm quartz cuvettes. Three spectra were averaged for each protein. To study the effect of pH, the spectra were collected in either 100 mM phosphate-citrate buffer or 100 mM phosphate buffer (pH 2.4 – 10.0) using 1-cm quartz cuvettes at room temperature. Buffer exchange was performed using a PD-10 column from GE Healthcare Life Sciences.

Ligand-binding study

Cyanide (CN^-) and carbon monoxide (CO) are known ligands for most heme-containing proteins including CPO.[37,38] The UV-Vis absorption spectra of ferric and ferrous mutant and WT CPO in 25 mM phosphate buffer, pH 6.0 in the absence and presence of the ligands were collected using 1-cm quartz cuvettes at room temperature. For CO binding, WT and mutant CPO were reduced with sodium dithionite and purged with CO for 1 minute.

In the CN^- binding study, the final concentration of cyanide in the samples was 100 mM. The spectra were collected upon initial addition of the anion ligand (0 min) and after 1-hour incubation (60 min) of the sample at room temperature. Titrations of CPO (3-8 µM) with CN^- (10-800 µM for WT and 1-10 mM for mutants) were performed in a phosphate buffer, pH 6.0. The cyanide dissociation constant (Kd), which is an inverse of a binding constant (K), was calculated using equation 1,[39] where ΔA is the maximum absorbance difference, ΔA∞ is the change in absorbance of CPO-CN complete formation, K

is a binding affinity constant, and [S] is the concentration of free CN^-:

$$1/\Delta A = (1/[S]) \times (1/(K\Delta A\infty)) + (1/\Delta A\infty) \quad \text{Eq. 1}$$

The Hill equation[40] was used to determine the stoichiometry of CN^- binding to the mutants, where h is the number of the binding sites:

$$\log(\Delta A/(\Delta A\infty - \Delta A)) = h \times \log[S] + \log(K) \quad \text{Eq. 2}$$

Enzymatic activity assays

All reactions were carried out in 1-cm quartz cuvettes containing a total of 3 ml of the reaction mixture composed of the appropriate concentrations of the buffer and substrates as described in each specific activity assay. All assays were initiated by the addition of hydrogen peroxide (except for the catalase assay) and monitored for 180 seconds with a UV/Vis spectrophotometer at room temperature. The initial rates of reactions were calculated from the linear portions of the reaction curves.

The peroxidase activity of CPO was measured by the oxidation of ABTS commonly used to estimate the peroxidation activity of heme peroxidases. The reaction system consisted of either WT (0.03-5.0 μM) or mutant CPO (0.03-0.2 μM) in 100 mM phosphate-citrate buffer at different pH (2.75, 3.0, 3.5, 4.0, 4.5, 5.0, 5.5, 6.0) containing 36.8 μM ABTS. After H_2O_2 (3.6 mM, final concentration) addition, the progress of the reaction was monitored for the formation of oxidized ABTS at 405 nm.[41]

The monochlorodimedone (MCD) assay was used to determine the chlorination activity of CPO that catalyzes the conversion of MCD into dichlorodimedone (DCD).[1] The reaction mixture consisted of either 0.005-0.05 μM WT or 0.6 μM mutant CPO in 100 mM phosphate-citrate buffer at different pH (2.75, 3.0, 3.5, 4.0, 4.5, 5.0) containing 20 mM KCl and 0.17 mM MCD. After H_2O_2 (2.2 mM, final concentration) addition, the reaction was monitored at 278 nm.[1]

The catalatic (dismutation) activity was measured by monitoring decomposition of hydrogen peroxide. The reaction system consisted of 0.05% hydrogen peroxide in 100 mM phosphate-citrate buffer (pH 3.0, 3.5, 4.0, 4.5, 5.0, 5.5). After either 0.5 μM WT or mutant CPO was added, the reaction was monitored at 240 nm.[42]

The styrene epoxidation assay[43] was performed in 100 mM phosphate-citrate buffer (pH 3.0, 4.0, 5.0, 6.0, 7.0, 8.0, 9.0, 10.0) containing 0.3 mM styrene and either 0.3 μM WT or mutant CPO. After addition of 2.2 mM H_2O_2, the reaction was monitored at 262 nm at which styrene absorbs. The extinction coefficient of styrene at 262 nm was determined to be 0.6225 ± 0.0781 $mM^{-1}cm^{-1}$ from the slope of a plot of absorbance versus concentration (Figure S3). Styrene was dissolved in 100 mM phosphate-citrate buffer, pH 3.25. Since styrene absorbance decreases with time due to its poor solubility in aqueous solutions, all solutions with styrene were freshly prepared for each trial.

Calculations of specific activities

Specific activities (SA) were calculated using equation 3 while the change in the amount of a substrate or product over time was calculated using equation 4, where A is absorbance, ε is the extinction coefficient at a specific wavelength, b is the length of the light pathway, and c is the concentration of the substrate or product. The extinction coefficient values for the substrates are listed in Table S3.

$$SA = (\mu mol\ substrate\ or\ product/sec) / (\mu mol\ enzyme) \quad \text{Eq. 3}$$

$$A = \varepsilon bc \quad \text{Eq. 4}$$

Results

Expression and purification

The expression levels of R26A CPO in *A. niger* were quite low, which necessitated large volumes of culture in order to obtain sufficient amount of the mutant CPO for proper characterization studies (approximately 6 mg of pure protein was obtained from 72-L cultures). After purification, the mutant protein contained both halo- and apoprotein. To improve incorporation of the heme into the R26A mutant, hemin or its precursor (δ-aminolevulinic acid) was added to some cultures grown at 25°C for three days to a final concentration of either 25 µM or 50 µM. However, addition of either hemin or its precursor failed to improve heme incorporation into R26A as determined from similar Rz values of the protein expressed with and without hemin or its precursor. Furthermore, R26A had lower overall

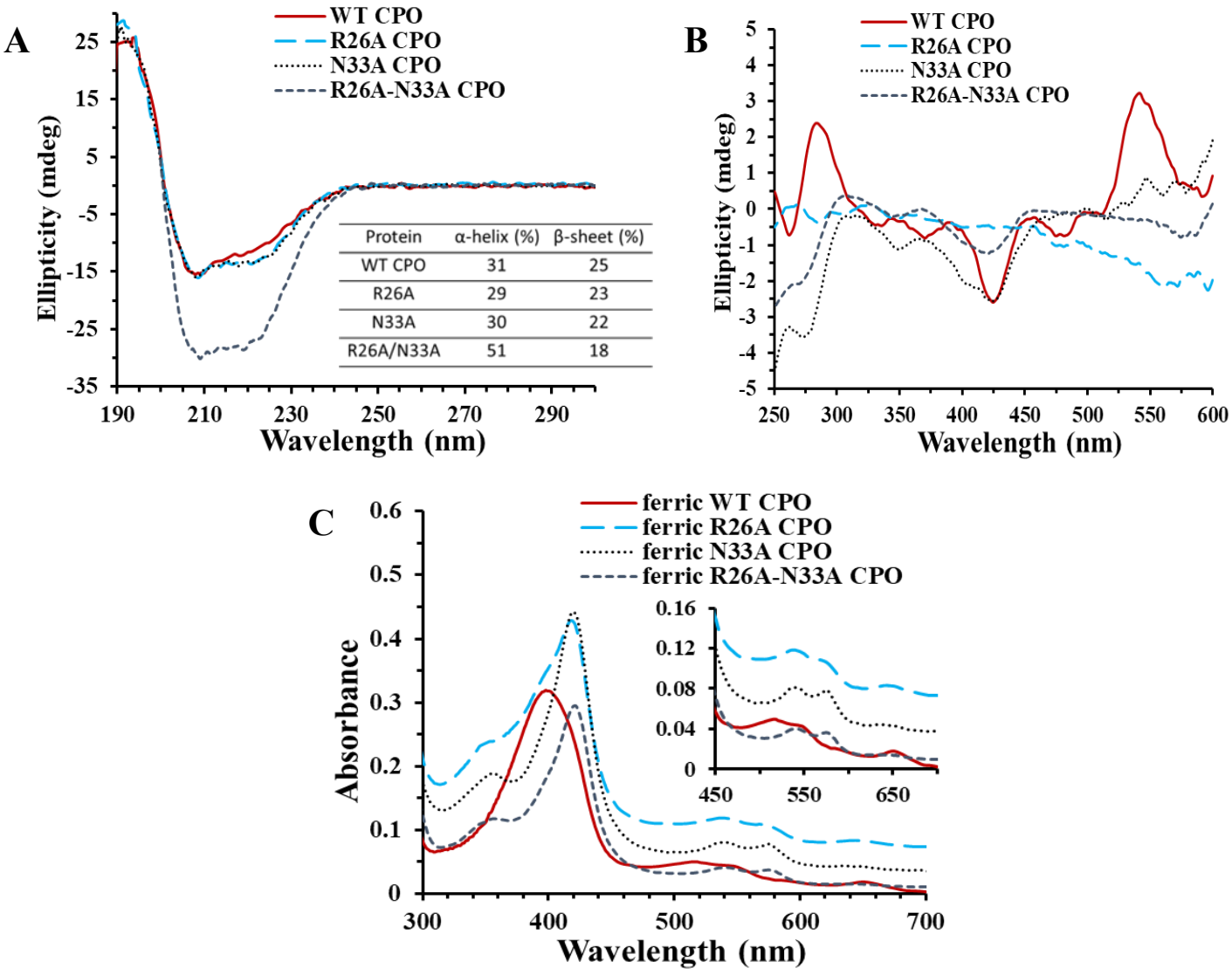

Figure 3. A. Secondary structure spectroscopic signatures of WT and mutant CPO in phosphate buffer, pH 5.9 and associated alpha-helical and beta-sheet content in the secondary structures. B. Tertiary structure spectroscopic signatures of WT and mutant CPO in phosphate buffer, pH 5.9. C. UV-Vis spectra of WT and mutant CPO in phosphate buffer, pH 5.9. Soret bands are located at 398 and 418, 420, and 421 nm, respectively. The insert shows an expansion of the visible region Q-bands of WT and mutant CPO.

stability than the WT or the other two mutant CPO proteins (N33A and R26A/N33A) as indicated by the significant decrease in the Soret band intensity of R26A within 1-2 months of protein expression (not shown).

Secondary and tertiary structures of the WT and mutant CPO proteins

Circular dichroism spectroscopy was used to verify whether a disruption of the hydrogen bonds between the Arg26-Asn37 and Ala27-Asn33 pairs individually and simultaneously had a significant effect on the secondary and tertiary structures of the enzyme, which in turn could affect catalysis and the ligand binding properties.

The CD spectral feature from 190 to 260 nm revealed the secondary structural information of the proteins. The essentially identical CD spectral pattern of WT, R26A, and N33A CPO shown in Figure 3A suggests that disrupting the hydrogen bonds between Arg26-Asn37 and Ala27-Asn33 individually have negligible effect on the secondary structure of CPO. However, the CD spectrum of R26A/N33A CPO is significantly different from that of the WT and the other two mutants. Using the CDSSTR method 33 and reference therein, the alpha-helical content was estimated for WT and all mutants (Figure 3A). The 1-2% difference between the secondary structures of the WT and single mutants is unlikely to significantly influence the tertiary structure and ligand binding or catalytic properties of CPO. However, removal of both pairs of H-bonds resulted in a noticeable alteration of the alpha-helix (20%-increase).

The CD spectra between 250 and 600 nm were used to evaluate the tertiary structure of the proteins (Figure 3B and Table S1). The signals in the 250-350 nm region arise from both the aromatic residues and disulfide bonds present in the protein. Trp, Tyr, and Phe absorb at around 290 nm, 280 nm, and 260-270 nm, respectively. In addition, the disulfide bond band extends from about 260 nm to its maximum at around 330 nm and typically produces a weak signal. However, its intensity depends on the C-S-S bond angle, dihedral angle of the disulfide bond, and the effects of the surrounding groups.[44,45]

Chloroperoxidase has 18 Phe, 5 Trp, and 11 Tyr in its primary structure. Thus, the broad positive signal in the 275-300 nm region observed for WT CPO is likely produced by the Trp and Tyr residues. The negative band at around 265 nm could be a combination of absorptions arising from Phe and a disulfide bond between Cys79 and Cys87. All three mutants produce negative signals in the aromatic region, which indicate changes in the rigidity or environment of the aromatic residues and possibly of the disulfide bond region.

The region between 400-600 nm provides information about the heme environment. Heme absorbs at around 350 nm (delta band), 410 nm (Soret), and between 500-600 nm (Q bands). In the CD spectrum of WT CPO, the heme group has strong absorptions at 428 nm (Soret) and 545 nm (Q band). Additional weak negative signals are located at 372 nm and 480 nm. The CD spectra of the mutants are markedly different from that of the WT (Figure 3B and Table S1). WT CPO has a positive signal in the aromatic region and two strong heme group signals at 428 nm (Soret) and 545 nm (Q band). These absorptions disappear in the spectrum of the R26A mutant that has a broad negative peak in the 500-600 nm region with two maxima at 561 nm and 572 nm. The CD spectrum of R26A suggests that the heme environment in R26A is quite different from that in the WT. In addition, the absence of the Soret signal may reflect poor incorporation of the heme into the R26A mutant, which is also supported by the lower RZ value. Furthermore, the Soret band in the R26A UV-Vis spectrum decreases significantly within 1-2 months of protein storage, indicating low mutant stability. A very weak signal

Table 1. UV-Vis spectral properties of ferric WT and mutant CPO and their cyanide complexes at pH 6.0

Protein	δ band (nm)	Soret (nm)	β band (nm)	α band (nm)	CT (nm)
WT CPO	--	398	515	550	650
WT-CN	364	439	--	564	--
R26A	354	418	540	568	644
R26A-CN	364	436→432	--	560	--
N33A	356	420	540	575	--
N33A-CN	364	437→427	--	557	--
R26A/N33A	356	421	540	575	644
R26A/N33A-CN	364	439→437	--	555	--

at around 344-350 nm (delta band) is present in the spectra of all three mutants, which indicates that the electronegative environment of the heme has changed in the H-bond deletion mutants. In the spectra of N33A and R26A/N33A, the Soret bands are observed at 424 nm and 420 nm, respectively, and are broader than that of the WT with a shoulder at around 400 nm. In the spectra of both N33A and R26A/N33A mutants, there are no signals at 370 nm and 480 nm; however, three and two Q bands are present, respectively. These observations suggest that the heme active centers in those two mutants are similar to each other but different from that in the WT.

Heme coordination and ligand binding to WT and mutant CPO

To further investigate the heme center of the mutants, UV-Vis measurements were taken for both WT and mutant CPO (Figure 3C). At pH 6.0, the WT spectrum shows, as expected, the Soret peak at 398 nm as well as the β, α, and CT bands (Figure 3C and Table 1). The high-spin markers at 515 nm and 650 nm indicate that the heme iron is in the high-spin pentacoordinated state. The spectroscopic signature of high-spin pentacoordinated WT CPO remains stable over the acidic and neutral pH range, shifting to a low-spin state at pH 8.0 and above (Figure 4A), which is consistent with previously reported data showing that transition to the alkaline low-spin, hexacoordinate form occurs between pH 7 and 8.[46]

The Soret, β, and α bands of the mutants are red-shifted (Table 1). These spectral features are consistent with the presence of a low-spin heme with a sixth ligand that can be either water or the side chain of an amino acid residue in the distal pocket. The presence of a CT band in the R26A and R26A/N33A spectra suggests that a small fraction of the protein may be in a high-spin state. Furthermore, the α/β band intensity ratio in the WT spectrum is similar to that in R26A and lower than that in the N33A and R26A/N33A mutant spectra. These ratios suggest that the a2u and a1u porphyrin orbitals in WT and R26A may be closer in energy than those in N33A and R26A/N33A. In addition, the spectra of all mutants possess a clear δ-band, which is also an indication of a low-spin heme.

The stability of the heme environment at different pH in the mutant CPO proteins is different from that in WT CPO with the double mutant being the most stable of the three mutants over a wide pH range (Figure 4B-D). To further examine the effect of the mutations on the heme environment of CPO, UV-Vis spectra of the mutant CPO proteins and their complexes with CO (Figure 5 and Table S2) and CN^- (Figure 6 and Table 1) were compared with those of the corresponding WT CPO. The absorption spectra of the ferrous mutant CPO proteins are fundamentally indistinguishable from that of the ferrous

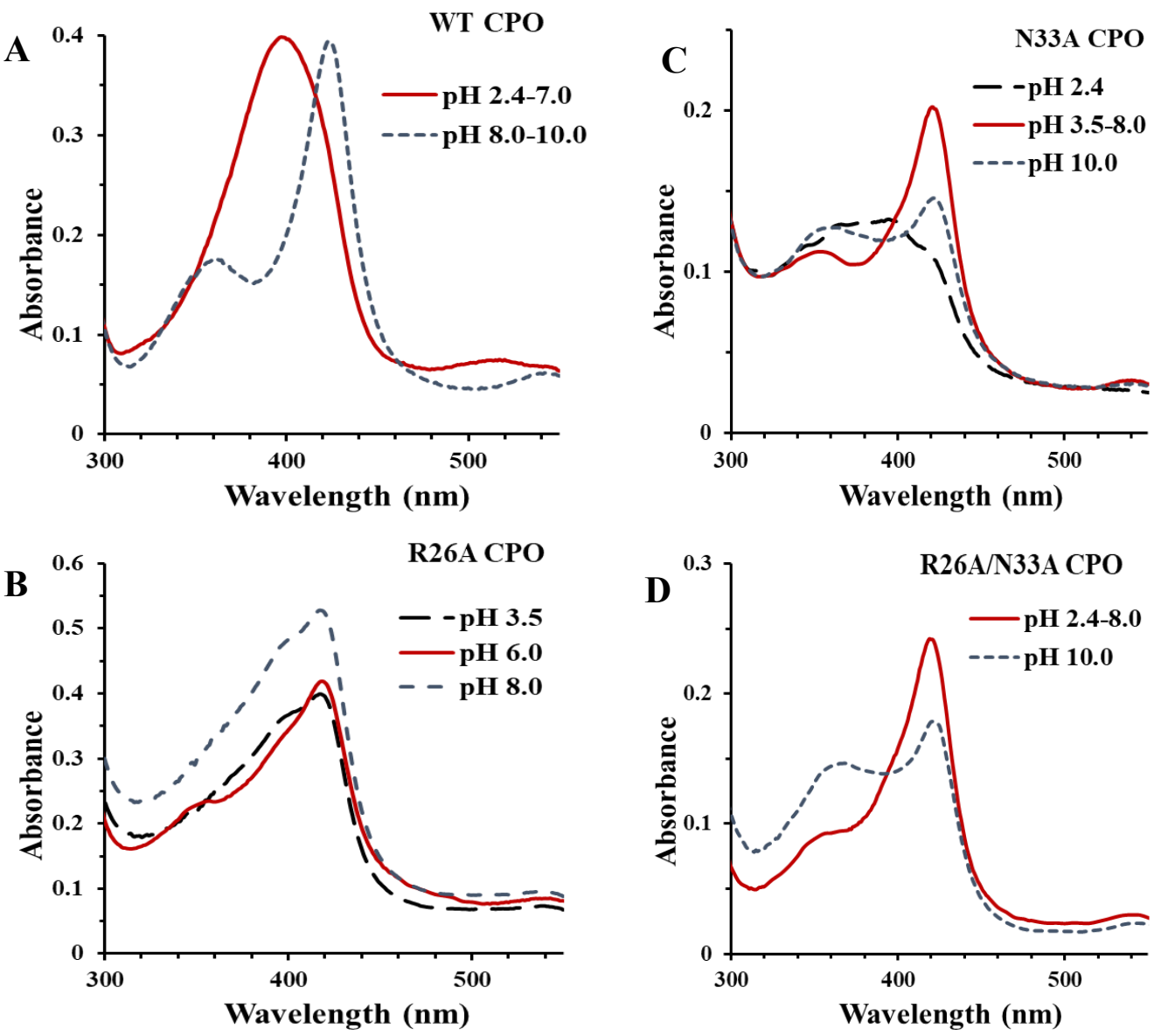

Figure 4. UV-Vis absorption spectra of WT (A) and mutant CPO (C-D) at various pH.

WT CPO with the Soret at 407-408 nm and Q-bands at 550-551 nm. Furthermore, the Soret absorption of the ferrous mutant CPO-CO complexes is also essentially identical to that of the WT CPO-CO adduct with the Soret bands at 444±1 nm. These spectral properties suggest that disrupting the proximal H-bonding network does not affect the binding of a strong neutral ligand, such as CO, to CPO. Interestingly, the N33A-CO and R26A/N33A-CO complexes show the delta band at 358 nm and 357 nm, respectively, with the first mutant having a more defined peak (Figure 5C, D). The presence of the delta band indicates differences in the electronegative environment of the heme in these two mutants, which can influence the catalytic properties of CPO.

The UV-Vis spectra of the ferric WT and mutant cyanide complexes were obtained at pH 6.0 (Figure 6) in the presence of CN^- excess. Interestingly, the spectral features of mutant CPO-CN gradually change with a slight Soret band blue-shift (Figure 6B-D and Table 1). No further spectral changes were observed beyond 1 hour of CN^- addition, indicating an equilibrium was reached. However, no spectral changes were observed for WT CPO-CN whose Soret band remained at 439 nm (Figure 6A), in

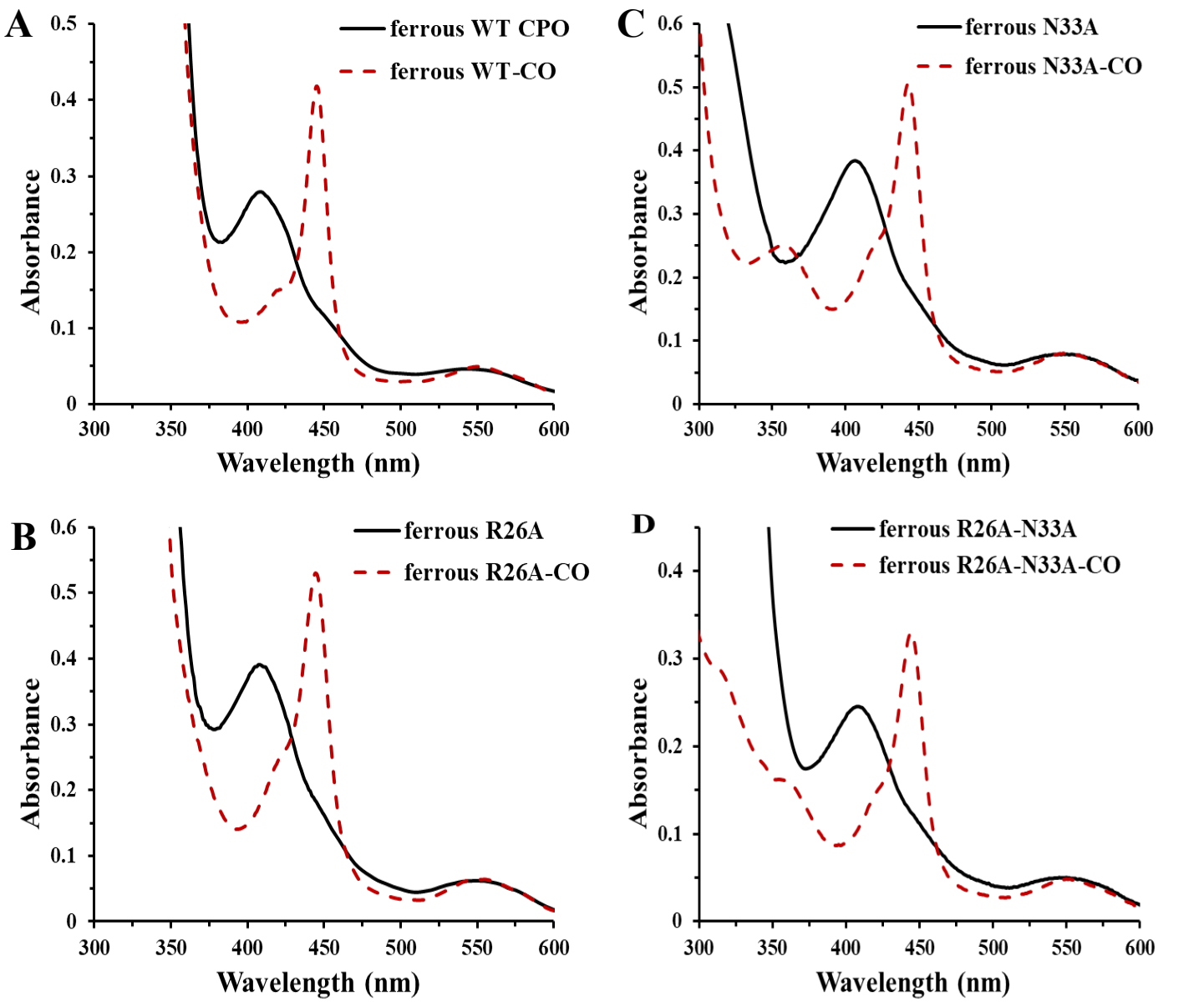

Figure 5. A. UV-Vis absorption spectra of ferrous WT CPO and ferrous WT-CO complex in phosphate buffer, pH5.9. B-D. UV-Vis absorption spectra of ferrous mutant CPO and ferrous mutant-CO complexes in phosphate buffer, pH5.9.

agreement with the observations reported previously.[47]

The slow binding equilibrium between free and cyanide-bound mutant CPO suggests that the sixth coordination site in the mutant CPO is occupied by either an H_2O molecule or an exogenous ligand. Therefore, cyanide has to compete with the existing axial ligand which hinders the speed of CN^- binding and may also result in a lower binding affinity for the mutant than WT CPO. To determine the cyanide dissociation constant, both the WT and mutant CPO proteins were titrated with potassium cyanide at pH 6.0 (Figure 7A-D). The presence of the isosbestic point in all CPO spectra is consistent with the equilibrium between the uncomplexed CPO and CPO-CN species. The Kd values were calculated using equation 1 (Figure 7E) and are listed in Table 2 indicating lower affinity of cyanide for the mutant CPO. The Kd result for the R26A mutant should be treated with caution since only one trial was performed because of the low yield and stability of this mutant. Decreased strength of CN^- binding to the mutants having a low-spin heme is consistent with a decreased CN^- affinity to the WT (Kd of 4 mM) having a low-spin heme at alkaline pH.[47] However, the WT and mutant low-spin forms must be

Table 2. Cyanide dissociation constants for CPO-CN complexes at pH 6.0.

Protein	CN^- Kd
WT CPO	130.0±6.5 μM
R26A	3.6 mM
N33A	10.5±1.0 mM
R26A/N33A	3.8±0.4 mM

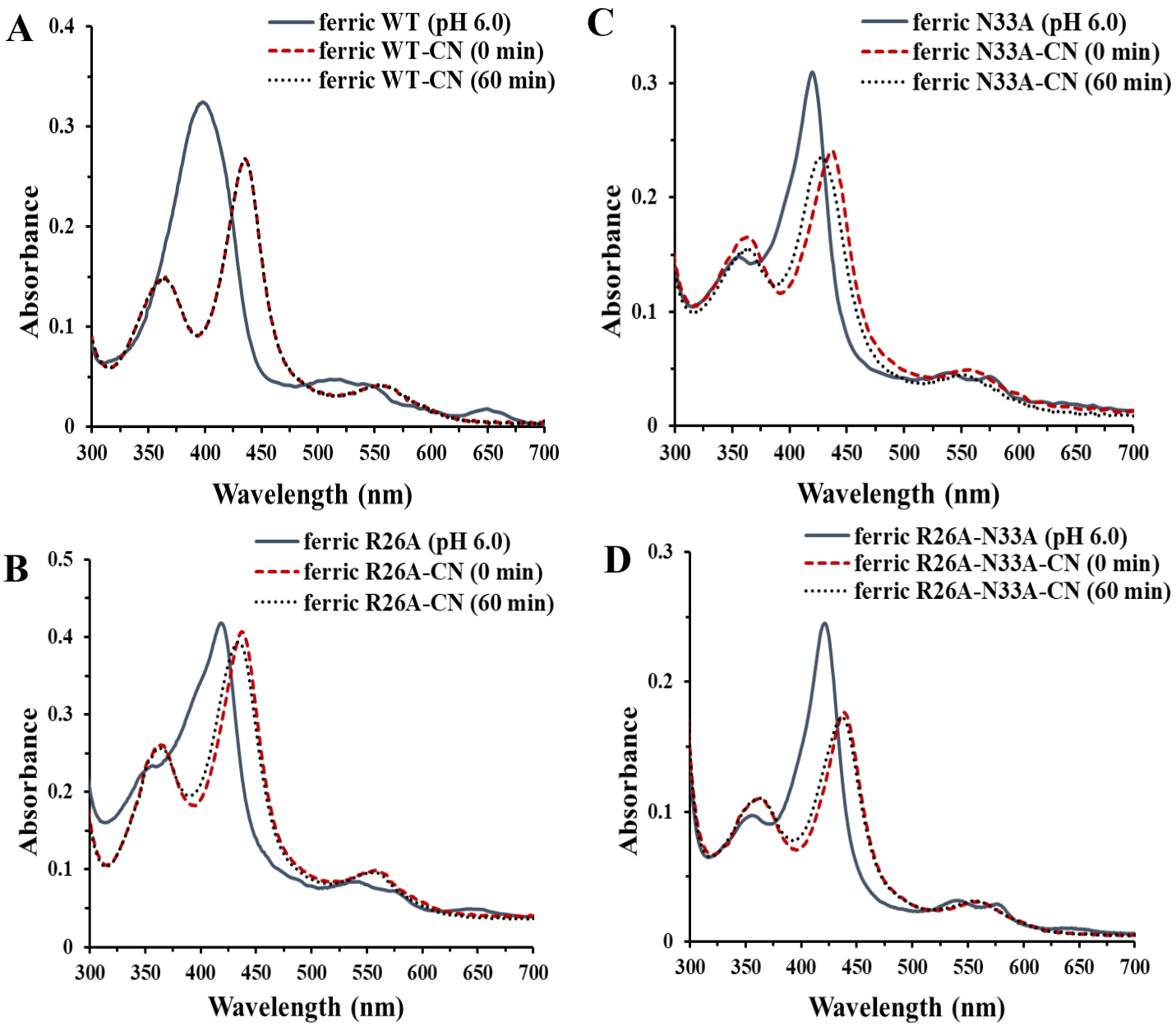

Figure 6. UV-Vis absorption spectra of ferric WT and WT-CN (A), ferric R26A and R26A-CN (B), ferric N33A and N33A-CN (C), ferric R26A/N33A and R26A/N33A-CN at pH 6.0 (D). 0-min spectra were taken immediately after CN- addition, 60-min spectra were taken after 1-hour incubation with CN-.

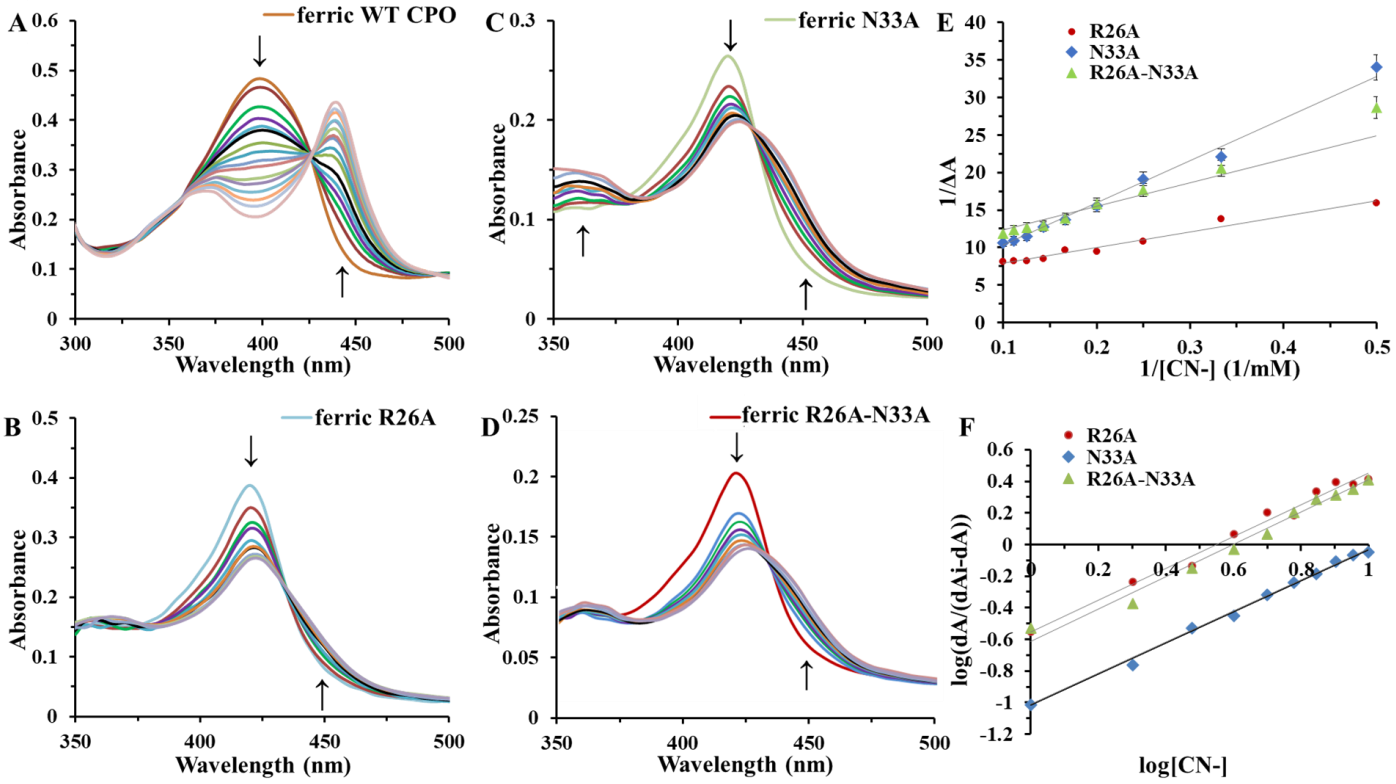

Figure 7. Titration of WT CPO (A), R26A (B), N33A (C), and R26A/N33A (D) with cyanide in phosphate buffer, pH 6.0. E. CN - Kd determination for the mutant CPO (Only 1 trial for R26A was performed because of the low yield and limited amount of the protein). F. The Hill plot (determination of mutant CPO-CN binding stoichiometry). The slopes of R26A, N33A, and R26A -N33A plots are 1.0048, 0.9943, and 1.0249, respectively.

different since the low-spin WT is enzymatically inactive, while the mutants are active. The Hill plot (Figure 7F) shows that CN^- binding to the R26A, N33A, and R26A/N33A mutants follows the same stoichiometry as in binding to the WT: one molecule of cyanide binds to one molecule of CPO.

Activities of mutant CPO as a function of pH

To examine the effect of hydrogen bond deletion between Arg26-Asn37 and Ala27-Asn33 on the catalytic properties of CPO, 4 enzymatic assays at various pH were performed: chlorination, dismutation, epoxidation, and peroxidation. WT CPO catalyzed chlorination reaction most efficiently at a very acidic pH with the optimal pH at 2.75 (Figure 8A) while the CPO mutants were essentially devoid of the chlorination activity in the tested pH range of 2.75-5.0, suggesting that Cpd X is likely to be responsible for the differences in the enzyme activities observed at various pH.

Hydrogen peroxide decomposition, a two-electron disproportionation reaction, is catalyzed by WT CPO most efficiently at acidic pH with the highest rate at pH 4.5-5.0 (Figure 8B). R26A CPO displayed catalatic activity of <6% at pH 4.5 and 5.0 and ≤2% at other tested pH compared to WT CPO. No catalatic activity was observed at any tested pH (3.0-5.5) in the N33A and R26A/N33A CPO mutants. Essentially absent catalatic activity of the mutant CPO suggested a reduction in the heme redox potential and/or an obstruction of H_2O_2 binding to Cpd I of the mutant CPO. The impaired disproportionation pathway eliminates the inevitable competition epoxidation has to deal with in WT CPO, overriding the adverse effect of a reduction in the heme redox potential and consequently conferring significantly enhanced epoxidation activity to the mutant CPO as observed in the

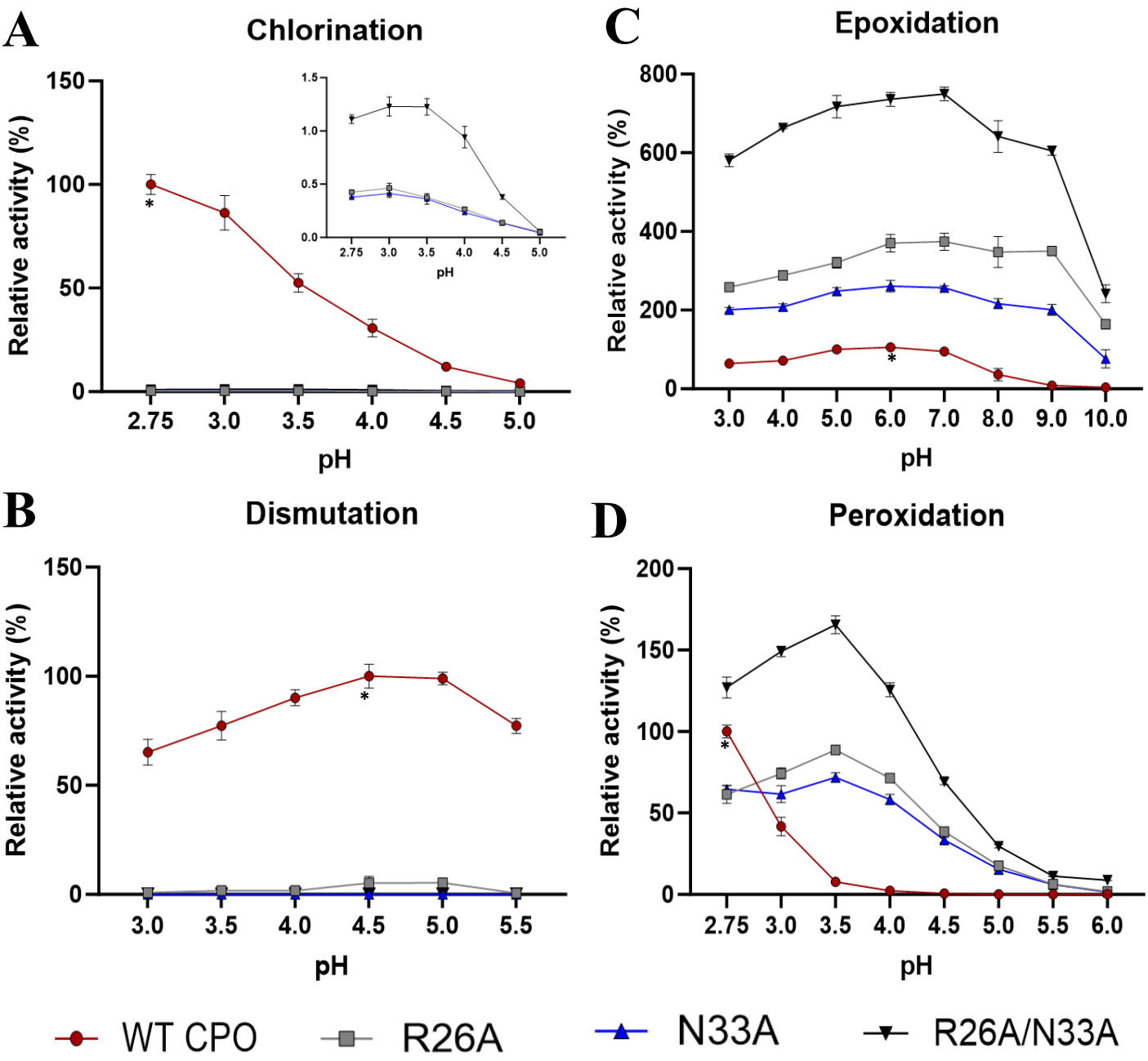

Figure 8. Relative catalytic activities of WT and mutant CPO: chlorination (A), dismutation (B), peroxidation (C), and epoxidation (D). * designates optimal activity of the WT and is taken to be 100%, other activities were calculated relative to the optimal activity of WT CPO.

epoxidation assay discussed next.

The rate of mutant CPO-catalyzed epoxidation of styrene was dramatically higher than that of WT CPO at all tested pH (3.0-10.0) (Figure 8C). Moreover, in the reactions catalyzed by the mutant CPO enzymes, styrene epoxidation does not seem to depend heavily on pH since mutant CPO oxidizes styrene at acidic, neutral, and basic pH with similar efficiency, except at pH 10.0, where the enzyme inactivation starts occurring (Figure 4C, D). A significant decrease in WT CPO activity is observed above pH 8.0 because of the formation of the inactive alkaline species of WT CPO (Figure 4A).[46] However, epoxidation catalyzed by the mutant CPO remained highly active at both pH8.0 and pH 9.0,

especially the R26A/N33A mutant (Figure 8C), suggesting that the mutant CPO did not form the inactive alkaline form in this pH range as WT CPO did (Figure 4A). This observation implies that Cpd I can be successfully generated in the mutant CPO over a broader pH range than in WT CPO.

The rate of peroxidation reaction catalyzed by WT CPO peaked at pH 2.75 and reduced sharply as pH was increased to 3.5 (Figure 8D). However, all mutant CPO proteins displayed the highest peroxidation activity at pH 3.5 and remained active even at pH 4.5 when WT CPO is devoid of the peroxidation activity, suggesting a possible increase in the pKa of Cpd II or the distal acid-base catalyst, E183.

Discussion

We explored the effects of a disruption of the hydrogen bonding network between R26-N37 and A27-N33 in the proximal pocket of CPO on its structural stability and catalytic profile. The essentially identical CD spectral patterns of WT, R26A, and N33A CPO suggest that disrupting the hydrogen bonds between R26-N37 and A27-N33 individually has a negligible effect on the secondary structure of CPO whereas simultaneous disruption of these hydrogen bonds changes the secondary structure of the enzyme by significantly increasing its alpha-helical content. Since the amino acids directly adjacent to the proximal helix are disordered (Figure 1), it is possible that the absence of the H-bonds promotes organization of this region into an alpha helix extending helix A affecting its rigidity and orientation. Such changes in the proximal helix would affect the local heme environment since Cys29, the heme ligand, is situated in this helix. Surprisingly, further CD and optical studies revealed striking differences between WT and all mutant CPO proteins in terms of the tertiary structure and catalytic properties. The dramatically different CD spectral patterns of the mutants compared to that of WT CPO indicate that removal of the H-bond pair between R26 and N37, and between A27 and N33 significantly affects the tertiary structure of CPO, and the heme environment has been altered in all three mutants, although the secondary structures are essentially maintained with the single mutations. Since the biochemical properties of proteins are mainly determined by their tertiary structure, we expected that the ligand-binding and catalytic properties of the mutant CPO enzymes would be significantly different from that of WT CPO, and explored these properties next.

The CO-binding properties of the CPO mutants are similar to that of the WT as evident from the fundamentally indistinguishable spectra of the WT CPO-CO and mutant CPO-CO complexes (Figure 5). These spectral properties suggest that disrupting the proximal H-bonds between R26 and N37, and between A27 and N33 does not affect the binding of a strong neutral ligand, such as CO, to CPO. Cyanide binding to the mutant CPO, however, exhibits a slower binding equilibrium and weaker binding compared to the WT CPO. Previous studies on ligand binding to CPO revealed that cyanide diffuses into the distal heme pocket in a protonated form, HCN, and loses its proton upon binding to the heme iron.[38,47] Since WT CPO has no distal ligand, HCN can bind to the heme more readily. In contrast, R26A, N33A, and R26A/N33A CPO have a low-spin ferric heme and likely possess water or another amino acid as a distal ligand that competes with CN^- for binding to the heme, which would explain a slower binding equilibrium and lower CN^- affinity for the mutant CPO (Table 2).

The catalytic profiles of the mutant CPO were significantly altered as well upon the proximal H-bond disruptions. The catalytic property of heme proteins is influenced by a plethora of intricate factors including but not limited to the heme iron redox potential, strength of electron pushing effects of the proximal ligand, basicity of the distal acid/base catalyst, and accessibility of the active site to substrates.[48-50] Additionally, the pKa of the protonated intermediates normally determines the optimal pH of catalysis. For example, the chlorination reaction catalyzed by WT CPO is most efficient at very

acidic pH with the optimal pH 2.75 (Figure 8A). Chlorination requires the formation of Cpd I and Cpd X.[25,30] Thus, the rate of chloride oxidation depends on the formation rates of the two intermediates. Since the rate of Cpd I formation has been shown to be independent of pH,[24,51] Cpd X is likely to be responsible for the differences in the activities observed at various pH. Indeed, it has been demonstrated that only protonated Cpd X is able to chlorinate MCD,[51] which explains WT CPO's high chlorination activity at acidic pH. In contrast, all mutant CPO proteins were practically devoid of chlorination activity in the tested pH range of 2.75-5.0 (Figure 8A). The loss of chlorination activity may be attributed to a decrease in the redox potential of Cpd I as implicated by the tertiary structural changes in the mutant CPO (Figure 3B) or the inability of Glu 183 to generate the protonated Cpd X that is required for chlorination. It is worth mentioning that the tertiary structural rearrangement induced by the mutation could have brought about changes in the heme exposure to the solvent that may also contribute to the decrease in the redox potential of Cpd I, which in turn, impairs the chlorination and catalatic activities of the enzyme.[52,53] This is consistent with a negligible dismutation activity of the mutants (Figure 8B) at different pH (3.0-5.5).

In contrast to the eliminated chlorination and dismutation activities in the mutant CPO proteins, the epoxidation and peroxidation activities were increased. The styrene epoxidation reaction is catalyzed more efficiently by the mutant CPO enzymes (especially the double mutant) compared to the WT CPO over a wide pH range (3.0-10.0). This result indicates that Cpd I can be successfully generated in the mutant CPO over a broader pH range than in WT CPO. The fact that both the WT and mutant CPO remained highly active in a wide pH range suggests that the rate limiting step in epoxidation does not require the protonation/deprotonation of a catalytic intermediate, as in the case of the chlorination and peroxidation reactions, or a direct oxygen transfer is involved. In fact, a direct oxygen transfer from Cpd I to a substrate has been proposed in CPO-catalyzed oxidation of indole.[54] As judged from the CD spectra (Figure 3A-B), another contribution to the increase in the epoxidation activity of the mutants may come from the changes in the accessibility of the active site by the substrates, which is important for two-electron oxidations by heme enzymes.[55] Large changes in the secondary structure of the double mutant (Figure 3A), having the highest epoxidation rates (Figure 8C), are consistent with an increased active site accessibility.

WT CPO catalyzes peroxidation reactions with the most efficiency at pH 2.75. It has been postulated that peroxidation proceeds through Cpd II, a hydroxyl ferryl intermediate.[21,56] High peroxidation activity at a very acidic pH is consistent with this hypothesis. However, the H-bond disruptions resulted in a shifted optimal pH for peroxidation from 2.75 to 3.5. Such shift suggests an increase in the pKa of Cpd II, thus allowing formation of the required intermediate at higher pH. On the other hand, the upshifted optimum pH of 3.5 for the mutant CPO compared with that of 2.75 for WT CPO may also implicate that the pKa of the distal acid-base catalyst, E183, was increased in the mutant due to the disruption of the proximal hydrogen bond network. The low pKa of E183 has been attributed to the unusually low pH range for WT CPO-catalyzed reactions.[2] The wider pH range over which the mutant CPO proteins remain active relative to WT CPO suggests that the mutations result in the global structural alterations (see CD results) that make the mutants less sensitive to pH changes.

The variations in the tertiary CD spectra of the mutant CPO proteins compared to that of WT CPO indicate significant global differences between the proteins. Surprisingly, these global alterations were not the consequences of the secondary structural changes in the single mutant CPO proteins as reflected by the nearly identical secondary CD spectrum of WT CPO to that of the R26A and N33A mutants. It is reasonable to infer from these results that removal of the R26-N37 or A27-N33 hydrogen bonds

destabilizes the orientation of the proximal alpha helix, which in turn, increases the electron donation of the axial thiolate and thus its "push" effect. The inability of the mutant CPO enzymes to catalyze chlorination and dismutation reactions is in good agreement with a previous report that an increased "push" effect in heme-thiolate proteins results in a reduction in the heme redox potential.[19] Although the reduction of the heme redox potential may be caused by various global changes that could impact, for instance, the polarity of the distal pocket, the most reasonable explanation for the observed effect is reorientation of the proximal helix. Small orientational changes would significantly reduce the influence of the helix dipole, resulting in a decrease in the heme redox potential, while large orientational changes are likely to break the amide hydrogen bonds between A31 and L32 to C29, leading to a more substantial reduction in the heme redox potential. However, breaking the amide hydrogen bonds would lead to the formation of an inactive species as the proximal Cys would be exposed to protonation. Since the formation of inactive CPO did not occur, as evidenced by the efficient epoxidation and peroxidation activities, it is likely that destabilization of the proximal alpha helix does not induce very large orientational alterations.

Conclusion

We have demonstrated that the hydrogen bonds between the side chains of R26-N37 and A27-N33 in the proximal heme pocket of CPO play a significant role in modulating the stability and catalytic profile of this versatile heme peroxidase as reflected by the significantly improved activity in alkali conditions and essentially obstructed chlorination and dismutation pathways coupled with the considerably enhanced peroxidation and epoxidation activities. Our results suggest that the disruption of the hydrogen bonds between R26-N37 or A27-N33 (individually) has negligible effects on the secondary structure of CPO while simultaneous disruption of these bonds significantly changes the secondary structure of the double-mutant CPO. However, these H-bonds, separately and together, are crucial to modulating the tertiary structure of the protein, regulating the stability of the heme-thiolate coordination, fine-tuning the acidity/basicity (pKa) of the distal acid/base catalyst (E183), and controlling the redox potential of the heme iron. This work is anticipated to contribute to the understanding of structure-function relationships of heme proteins in general and the structural basis for the broad spectrum of the activities displayed by CPO in particular.

Acknowledgments

This research was supported by the National Science Foundation under Award No CHE-0540763 to X.W. (CAREER Award).

We wish to thank Ana Recinos-Baez and Elwood Kwong for help with protein expression.

Present address of E. S.: Department of Surgery, University of Miami, Miami, FL 33136, USA

Conflict of interest

The authors declare no conflict of interest.

Affiliations

Department of Chemistry and Biochemistry, Florida International University, Miami, FL 33199, USA

Supplementary Material

Supplementary Material

References

1. Hager LP, Morris DR, Brown FS, Eberwein H. (1966) Chloroperoxidase. II. Utilization of Halogen Anions. Journal of Biological Chemistry. 241(8), 1769-1777.
2. Sundaramoorthy M, Terner J, Poulos TL. (1995) The Crystal Structure of Chloroperoxidase: A Heme Peroxidase-Cytochrome P450 Functional Hybrid. Journal of Inorganic Biochemistry. 59(2 –3), 427.
3. Zamocky M, Furtmüller PG, Obinger C. (2008) Evolution of Catalases from Bacteria to Humans. Antioxidants & Redox Signaling. 10(9), 1527-1548.
4. Hansberg W. (2022) Monofunctional Heme-Catalases. Antioxidants. 11(11), 2173.
5. Zámocký M, Hofbauer S, Schaffne, I, Gasselhuber B, Nicolussi A et al. (2015) Independent Evolution of Four Heme Peroxidase Superfamilies. Archives of Biochemistry and Biophysics. 574, 108-119.
6. Lakner FJ, Cain KP, Hager LP. (1997) Enantioselective Epoxidation of ω-Bromo-2-Methyl-1 -Alkenes Catalyzed by Chloroperoxidase. Effect of Chain Length on Selectivity and Efficiency. Journal of the American Chemical Society. 119(2), 443-444.
7. Doerge DR, Corbett MD. Peroxygenation Mechanism for Chloroperoxidase-Catalyzed N -Oxidation of Arylamines. Chemical Research in Toxicology. 4(5), 556-560.
8. Bhandari Y, Sajwan H, Pandita P, Koteswara Rao V. (2022) Chloroperoxidase Applications in Chemical Synthesis of Industrial Relevance. Biocatalysis and Biotransformation. 41(6), 403-420.
9. Hollenberg PF, Hager LP. (1973) The P-450 Nature of the Carbon Monoxide Complex of Ferrous Chloroperoxidase. Journal of Biological Chemistry. 248(7), 2630-2633.
10. Yi X, Conesa A, Punt PJ, Hager LP. (2003) Examining the Role of Glutamic Acid 183 in Chloroperoxidase Catalysis. Journal of Biological Chemistry. 278(16), 13855-13859.
11. Yi X, Mroczko M, Manoj KM, Wang X, Hager LP. (1999) Replacement of the Proximal Heme Thiolate Ligand in Chloroperoxidase with a Histidine Residue. Proceedings of the National Academy of Sciences USA. 96(22), 12412-12417.
12. Roos G, Harvey JN. (2021) Histidine versus Cysteine-Bearing Heme-Dependent Halogen Peroxidases: Parallels and Differences for Cl- Oxidation. Journal of Physical Chemistry B. 125(1), 74-85.
13. Pardillo AD, Morozov AN, Chatfield DC. (2015) Proximal Pocket Hydrogen Bonds Significantly Influence the Mechanism of Chloroperoxidase Compound I Formation. Journal of Physical Chemistry B. 119(39), 12590-12602.
14. Morozov AN, Pardillo AD, Chatfield DC. (2015) Chloroperoxidase-Catalyzed Epoxidation of Cis-β-Methylstyrene: NH-S Hydrogen Bonds and Proximal Helix Dipole Change the Catalytic Mechanism and Significantly Lower the Reaction Barrier. Journal of Physical Chemistry B. 119 (45), 14350-14363.
15. Ogliaro F, de Visser SP, Shaik S. (2002) The 'Push' Effect of the Thiolate Ligand in Cytochrome P450: A Theoretical Gauging. Journal of Inorganic Biochemistry. 91(4), 554-567.
16. Sono M, Roach MP, Coulter ED, Dawson JH. (1996) Heme-Containing Oxygenases. Chemical Reviews. 96(7), 2841-2888.

17. Groves JT. (2014) Enzymatic C-H Bond Activation: Using Push to Get Pull: Enzymatic C-H Bond Activation. Nature Chemistry. 6(2), 89-91.

18. Harris DL, Loew GH.(1998) Theoretical Investigation of the Proton Assisted Pathway to Formation of Cytochrome P450 Compound I. Journal of the American Chemical Society. 120(35), 8941-8948.

19. Yoshioka S, Tosha T, Takahashi S, Ishimori K, Hori H et al. (2002) Roles of the Proximal Hydrogen Bonding Network in Cytochrome P450cam-Catalyzed Oxygenation. Journal of the American Chemical Society. 124(49), 14571-14579.

20. Dey A, Jiang Y, Ortiz de Montellano P, Hodgson KO, Hedman B et al. (2009) S K-Edge XAS and DFT Calculations on Cytochrome P450: Covalent and Ionic Contributions to the Cysteine-Fe Bond and Their Contribution to Reactivity. Journal of the American Chemical Society. 131(22), 7869-7878.

21. Green MT, Dawson JH, Gray HB. (2004) Oxoiron(IV) in Chloroperoxidase Compound II Is Basic: Implications for P450 Chemistry. Science. 304(5677), 1653-1656.

22. Ueno T, Kousumi Y, Yoshizawa-Kumagaye K, Nakajima K, Ueyama N et al. (1998) Role of α-Helix Conformation Cooperating with NH···S Hydrogen Bond in the Active Site of Cytochrome P-450 and Chloroperoxidase: Synthesis and Properties of [MIII(OEP)(Cys-Helical Peptide)] (M = Fe and Ga). Journal of the American Chemical Society. 120(47), 12264-12273.

23. Poulos TL, Finzel BC, Howard AJ. (1987) High-Resolution Crystal Structure of Cytochrome P450cam. Journal of Molecular Biology. 195(3), 687-700.

24. Hager LP, Doubek DL, Silverstein RM, Hargis JH, Martin JC. (1972) Chloroperoxidase. IX. Structure of Compound I. Journal of the American Chemical Society. 94(12), 4364-4366.

25. Wagenknecht HA, Woggon WD. (1997) Identification of Intermediates in the Catalytic Cycle of Chloroperoxidase. Chemical Biology. 4(5), 367-372.

26. Lambeir AM, Dunford HB, Pickard MA. (1987) Kinetics of the Oxidation of Ascorbic Acid, Ferrocyanide and p-Phenolsulfonic Acid by Chloroperoxidase Compounds I and II. European Journal of Biochemistry. 163(1), 123-127.

27. Manoj KM, Hager LP. (2008) Chloroperoxidase, a Janus Enzyme. Biochemistry. 47(9), 2997-3003.

28. Osborne RL, Raner GM, Hager LP, Dawson JH. (2006) C. Fumago Chloroperoxidase Is Also a Dehaloperoxidase: Oxidative Dehalogenation of Halophenols. Journal of the American Chemical Society. 128(4), 1036-1037.

29. Osborne RL, Coggins MK, Terner J, Dawson JH. (2007) Caldariomyces Fumago Chloroperoxidase Catalyzes the Oxidative Dehalogenation of Chlorophenols by a Mechanism Involving Two One-Electron Steps. Journal of the American Chemical Society. 129(48), 14838 -14839.

30. Murali Manoj K. (2006) Chlorinations Catalyzed by Chloroperoxidase Occur via Diffusible Intermediate(s) and the Reaction Components Play Multiple Roles in the Overall Process. Biochimica et Biophysica Acta. 1764(8), 1325-1339.

31. Hofrichter M, Kellner H, Pecyna MJ, Ullrich R. (2015) Fungal Unspecific Peroxygenases: Heme-Thiolate Proteins That Combine Peroxidase and Cytochrome P450 Properties. Advances in

Experimental Medicine and Biology. 851, 341-368.

32. Casella L, Gullotti M, Ghezzi R, Poli S, Beringhelli T et al. (1992) Mechanism of Enantioselective Oxygenation of Sulfides Catalyzed by Chloroperoxidase and Horseradish Peroxidase. Spectral Studies and Characterization of Enzyme-Substrate Complexes. Biochemistry. 31(39), 9451-9459.
33. Conesa A, van de Velde F, van Rantwijk F, Sheldon RA, van den Hondel CAMJJ et al. (2001) Expression of the Caldariomyces FumagoChloroperoxidase in Aspergillus Niger and Characterization of the Recombinant Enzyme. Journal of Biological Chemistry. 276(21), 17635 -17640.
34. Punt PJ, van den Hondel CA. (1992) Transformation of Filamentous Fungi Based on Hygromycin B and Phleomycin Resistance Markers. Methods in Enzymology. 216, 447-457.
35. Hutner SH, Provasoli L, Schatz A, Haskins CP. (1950) Some Approaches to the Study of the Role of Metals in the Metabolism of Microorganisms. Proceedings of the American Philosophical Society. 94(2), 152-170.
36. Whitmore L, Wallace BA. (2004) DICHROWEB, an Online Server for Protein Secondary Structure Analyses from Circular Dichroism Spectroscopic Data. Nucleic Acids Research. 32 (Web Server issue), W668-73.
37. Campbell BN Jr, Araiso T, Reinisch L, Yue KT, Hager LP. (1982) A Kinetic Study of the Binding of Carbon Monoxide to Ferrous Chloroperoxidase. Biochemistry. 21(18), 4343-4349.
38. Lambeir AM, Heremans K, Dunford HB. (1983) High-Pressure Effect on the Equilibrium and Kinetics of Cyanide Binding to Chloroperoxidase. Biophysical Chemistry. 18(3), 195-201.
39. Casella L, Gullotti M, Poli S, Bonfa M, Ferrari RP et al. (1991) Spectroscopic and binding studies on the stereoselective interaction of tyrosine with horseradish peroxidase and lactoperoxidase. Biochemical Journal. 279, 245-250.
40. Hill AV. (1910) The possible effects of the aggregation of the molecules of haemoglobin on its dissociation curves. The Journal of Physiology. 40, 389-403.
41. Childs RE, Bardsley WG. (1975) The Steady-State Kinetics of Peroxidase with 2,2'-Azino-Di-(3 -Ethyl-Benzthiazoline-6-Sulphonic Acid) as Chromogen. Biochemical Journal. 145(1), 93-103.
42. Aebi H. (1984) Catalase in Vitro. Methods in Enzymology. 105, 121-126.
43. Ortiz de Montellano PR, Choe YS, DePillis G, Catalano CE. (1987) Structure-Mechanism Relationships in Hemoproteins. Oxygenations Catalyzed by Chloroperoxidase and Horseradish Peroxidase. Journal of Biological Chemistry. 262(24), 11641-11646.
44. Kay E, Strickland EH, Billups C. (1974) Near Ultraviolet Circular Dichroism and Absorption Spectra of Chicken Ovomucoid and Acetylated Derivatives at 297 and 77 Degrees K. Journal of Biological Chemistry. 249(3), 797-802.
45. Kelly SM, Price NC. (2000) The Use of Circular Dichroism in the Investigation of Protein Structure and Function. Current Protein & Peptide Science. 1(4), 349-384.
46. Blanke SR, Martinis SA, Sligar SG, Hager LP, Rux JJ et al. (1996) Probing the Heme Iron Coordination Structure of Alkaline Chloroperoxidase. Biochemistry. 35(46), 14537-14543.
47. Sono M, Dawson JH, Hall K, Hager LP.(1986) Ligand and Halide Binding Properties of Chloroperoxidase: Peroxidase-Type Active Site Heme Environment with Cytochrome P-450 Type

Endogenous Axial Ligand and Spectroscopic Properties. Biochemistry. 25(2), 347-356.

48. Cusanovich MA, Hazzard JT, Meyer TE, Tollin G. (1989) Electron Transfer Mechanisms in Heme Proteins. Journal of Macromolecular Science, Part A. 26(2–3), 433-443.
49. Kersten PJ, Kalyanaraman B, Hammel KE, Reinhammar B, Kirk TK. (1990) Comparison of Lignin Peroxidase, Horseradish Peroxidase and Laccase in the Oxidation of Methoxybenzenes. Biochemical Journal. 268(2), 475-480.
50. Hong F, Jönsson LJ, Lundquist K, Wei Y. (2006) Oxidation Capacity of Laccases and Peroxidases as Reflected in Experiments with Methoxy-Substituted Benzyl Alcohols. Applied Biochemistry and Biotechnology. 129-132, 303-319.
51. Choudhury K, Sundaramoorthy M, Hickman A, Yonetani T, Woehl E et al. (1994) Role of the Proximal Ligand in Peroxidase Catalysis. Crystallographic, Kinetic, and Spectral Studies of Cytochrome c Peroxidase Proximal Ligand Mutants. Journal of Biological Chemistry. 269(32), 20239-20249.
52. Stellwagen E. (1978) Haem Exposure as the Determinate of Oxidation-Reduction Potential of Haem Proteins. Nature. 275(5675), 73-74.
53. Furtmüller PG, Zederbauer M, Jantschko W, Helm J, Bogner M et al. (2006) Active Site Structure and Catalytic Mechanisms of Human Peroxidases. Archives of Biochemistry and Biophysics. 445 (2), 199-213.
54. Zhang R, He Q, Chatfield D, Wang X. (2013) Paramagnetic Nuclear Magnetic Resonance Relaxation and Molecular Mechanics Studies of the Chloroperoxidase-Indole Complex: Insights into the Mechanism of Chloroperoxidase-Catalyzed Regioselective Oxidation of Indole. Biochemistry. 52(21), 3688-3701.
55. Harris RZ, Newmyer SL, Ortiz de Montellano PR. (1993) Horseradish peroxidase-catalyzed two-electron oxidations. Oxidation of iodide, thioanisoles, and phenols at distinct sites. Journal of Biological Chemistry. 268, 1637-1645.
56. Lai W, Chen H, Shaik S. (2009) What Kinds of Ferryl Species Exist for Compound II of Chloroperoxidase? A Dialog of Theory with Experiment. Journal of Physical Chemistry B. 113 (22), 7912-7917.